

Materials Design for Corrosion Rate Control in PM AZ91 Mg Alloy by Fe Addition[†]

KARIYA Shota*, JUNKO Umeda**, IMAI Hisashi**, KONDOH Katsuyoshi***, HARUO Unosawa****, Manuel Marya****

Abstract

Multi-stage hydraulic fracturing is a well-stimulation or hydrocarbon production enhancement process in which rock formation are fractured within isolated hydrocarbon well zones due to the injection of viscous liquids carrying propane gas. An important piece of hardware in multistage fracturing to create a temporary seal between hydrocarbon producing zones is a so-called a frac ball. Today, frac balls are most often made of reinforced polymers and are therefore greatly limited in pressure and temperature, indirectly restricting the number of stages per well that may be stimulated. As alternate to polymers, magnesium (Mg) and its alloys may be engineered for greater strength at rock formation temperatures, and the normally considered deficiency of magnesium and its alloys such as a limited corrosion resistance may be now advantageously used to create eco-friendly and fully degradable frac balls. Utilizing galvanic corrosion as a general principle to accelerate and control corrosion, magnesium may be used in combination with normally considered transition- metal impurities such as iron (Fe). However, the presence of iron in magnesium and its alloys is also known to influence mechanical properties adversely. Therefore, the relationships between Fe content, corrosion resistance, and mechanical properties still remain to be established for a specific manufacturing and heat treatment process. In this particular study, samples of AZ91 (Mg-9% Al-1% Zn) having various levels of iron were fabricated utilizing spark plasma sintering (SPS). Both compressive properties and corrosion rates were investigated and correlated to iron content.

KEY WORDS: (Magnesium), (Iron), (AZ91), (Galvanic corrosion)

1. Introduction

Shale gas and tight oil have received considerable attention in the last few years as a supplementary source of unconventional hydrocarbons to be introduced to the world production. Specifically oil and gas sources trapped within shale formations have remained largely inaccessible because of the low permeability of the shale rocks, and until recently have not been viable sources of hydrocarbons [1]. However, hydraulic fracturing in deviated wells is a method of creating passageways for the hydrocarbons to reach the well, and the recent progresses in multi-stage fracturing stimulation have made shale hydrocarbons far more attractive, particularly in North America [1]. In hydraulic fracturing, the rock formation is simply fractured by a hydraulically pressurized liquid carrying so-called proppants that keep the fracture opened for subsequent hydrocarbon production. In multistage hydraulic fracturing, the wellbore is divided into stages, and each stage is sequentially fractured after another utilizing hydraulic

pressure. To create the temporary seals between stages necessary for the fracturing of each zone, polymer balls are typically pumped down from the surface and upon landing onto pre-positioned receptacles create this temporary zone isolation [2]. Once a specific zone is fractured, the frac balls are normally displaced by the production flow; however, there is always an adverse risk that frac balls will remain trapped and therefore obstruct subsequent production in above zones closer to the wellhead [3]. A frac ball made of a degradable material would eliminate this concern, and therefore be appealing to the oilfields. Specifically, a frac ball advantageous to today's multistage fracturing would need to have a well-tuned degradability (i.e., a controllable corrosion rate), yet an enhanced mechanical strength at reservoir temperatures over today's polymeric balls. With these new and improved properties, not only greater operational temperatures may be eventually reached using drop ball frac systems, but also a greater number of stages may be treated, which in turns comes down to an

[†] Received on

* Graduate Student

** Assistant Professor

*** Professor

**** Schlumberger Limited Co., Ltd

Transactions of JWRI is published by Joining and Welding Research Institute, Osaka University, Ibaraki, Osaka 567-0047, Japan

improved hydrocarbon production recovery.

Magnesium (Mg) and its alloys have already found numerous applications in structural and mechanical components in part due to excellent combinations of low density and high mechanical properties. However, a disadvantage of magnesium that has restricted its applications has been its corrosion resistance, inferior to most engineering alloys [4]. Pure magnesium has a standard electrode potential of -2.36 V, which compared with other metals, in particular transition metals such as iron (Fe) and nickel (Ni) for instance, is much lower [5-6]. This directly infers that physical contact between magnesium and other dissimilar metals in the presence of a conductive liquid such as water will give rise to significant differences in potentials with magnesium by default on the anodic side of the resulting galvanic cell [7]. The greater the difference of electrode potential, the more severe is the resulting corrosion on the anodic sites, here made of magnesium or magnesium solid solutions [8-9]. As conventional alloy making practice, transition metals such as iron, nickel, as well as other metals that possess much greater electrode standard potential and are not metallurgically bound as inert intermetallic compounds are therefore commonly removed and left down to only ppm levels in commercial magnesium alloys. Conversely, in this short study, iron was purposely added to an AZ91 powder-metallurgy alloy to both increase and control corrosion in AZ91. The effect of iron addition on the resulting mechanical properties of the formed composite materials were investigated and related to the iron content in the formed materials.

2. Experimental

An AZ91 alloy (Mg, 9 wt. % Al, 1wt. % Zn) SWAP (Spinning Water Atomization Process) powder characterized by an average particle size of 514 μm was acquired for this study from a local powder producer Epson atmix corp. The AZ91 powder chemical composition was certified as follows: 9.02 wt.% Al, 0.65 wt.% Zn, 0.22 wt.% Mn, 0.05 wt.% Si, 0.01wt% Cu, 0.01 wt.% Fe and 0.01 wt.% Ni. For comparison purposes against further processed powders, Figure 1 (a) shows this as-received powder, overall quite coarse and tortuous in appearance. In order to accelerate the AZ91 corrosion, pure iron (Fe) powder with an average particle size of only 96 μm was also acquired and blended with the AZ91 powder. The as-received iron powder is revealed in Figure 1 (b), shown on the right of Figure 1 (a). To improve the dispersion of iron within the AZ91 and thus later promote uniform and predictable corrosion rates, the AZ91 SWAP powder was further crushed using a stamping mill (ANS-143, NITTO KAGAKU UCO, Ltd) operating for 60 min at 90 rpm, then sieved with 250 μm mesh (200 x 60 x 250 μm , AS ONE corporation). This subsequent processing resulted in a powder with average particle size estimated in the vicinity of 173 μm . Figure 1 (c) shows this new and finer powder for comparison purpose against Figures 1(a) and (b). This new and finer AZ91 SWAP powder, itself blended with 0.1, 0.5, 1 and

10 wt.% iron powder, was subsequently consolidated into 42 mm diameter billets using a fast and potentially economical process such as spark plasma sintering (SPS, SPS-1030, SPS Syntax). All samples were sintered at 673 deg K for 30 min and under 30 MPa inert gas pressure preceded by a short vacuum (6 Pa) to create inert sintering conditions. Following spark plasma sintering, the billets were hot-forged at 3 mm/sec using a 2000 kN hydraulic press (SHP-200-450, Shibayamakikai Co.) in order to maximize consolidation. Prior to forging, the billets were heated to 673 deg K for 5 min in argon protective atmosphere (RHL-P610C, ULVAC). Billet diameters pre and post forgings were 42 mm and 43mm, respectively.

Following conventional metallographic sample preparation, microstructural examinations were conducted using optical microscopy (Olympus DSX-500) and scanning electron microscopy (Jeol JSM-6500F). Mechanical properties were evaluated solely using compression tests on 4mm diameter and 10mm long samples. All compression tests were executed using a universal testing machine (Autograph AG-X 50 kN, Shimadzu) at an approximate quasi-static strain rate of 5×10^{-4} per sec. All tests were repeated a minimum of three times to validate the measurements.

Corrosion rates were estimated using simple immersion tests in 3.5wt. % magnetically stirred potassium chloride (KCl) solution at 303 deg. K. Weight measurements were completed on cubic samples of initial dimensions 10 x 10 x 10 mm after 30, 150 and 1500 min respectively. Prior to immersion, all test samples were silicon carbide ground to offer an identical and smooth surface finish. Complementarily, surface potential differences (SPD) between the main magnesium phase, α -Mg, and Fe-rich phases were also determined from measurements of surface potential against the tip of a PtIr5 cantilever attached to an SKPFM (Scanning Kelvin Probe Force Microscopy).

3. Results

Figure 2 shows billet cross-section microstructures in un-etched condition for 5 forged alloys, including 4 iron-enriched alloy composites. These are: (a) iron-free AZ91 (i.e., no iron added), (b) AZ91 with 0.1 wt.% Fe, (c) AZ91 with 0.5 wt.% Fe, (d) AZ91 with 1 wt.% Fe and (e) AZ91 with 10 wt.% Fe. First note that iron, being fully insoluble in magnesium is micro-segregated along internal boundaries, as described from the binary Mg (hcp) – Fe (bcc) phase diagram. Also note that the iron particles are fairly randomly distributed within the AZ91-Fe forged composite, a likely explanation being the sintering process. Following chemical etching, grain sizes in all 5 materials were observed to be relatively fine, seemingly in 4 to 5 μm , thereby indicating that iron in AZ91 has no measurable effect on grain size and is therefore not a source of Hall-Petch strengthening.

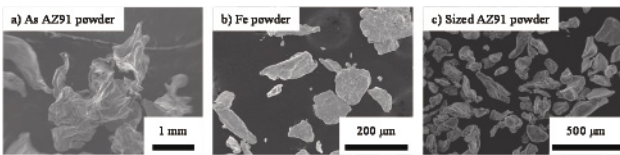


Fig. 1 SEM observation on as received AZ91 powder (a), Fe powder (b) and Sized AZ91 powder (c).

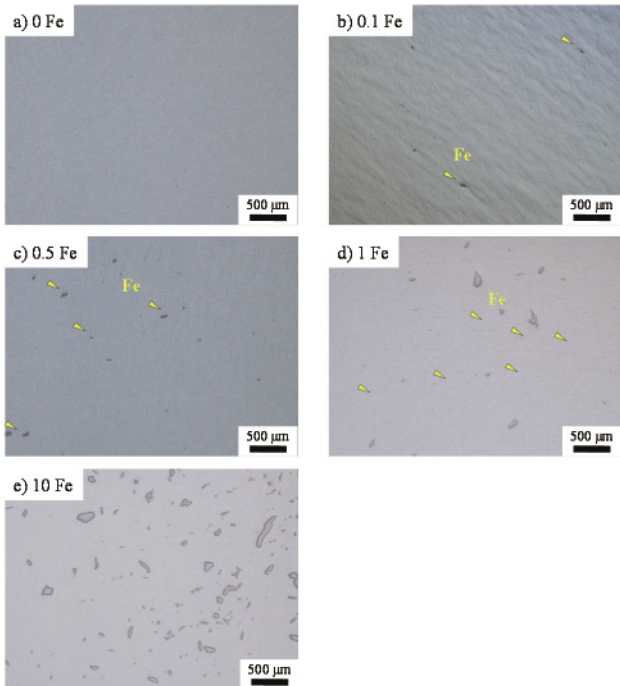


Fig. 2 Optical microscope observation on cross section of AZ91 composite forged composites with Fe content of 0 wt.% (a), 0.1 wt.% (b), 0.5 wt.% (c), 1 wt.% (d) and 10 wt.% (e).

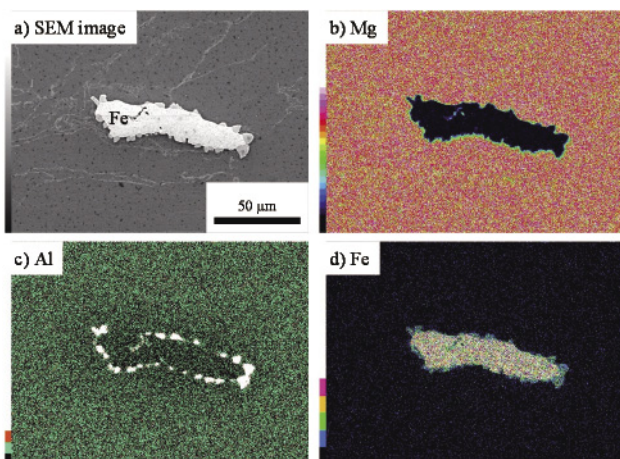


Fig. 3 SEM-EDS observation Fe particle of AZ91-10 wt. % Fe forged composite.

Figure 3 shows a set of SEM EDS maps for a randomly selected iron particle observed in the AZ91-10 wt. % Fe alloy composite. Also note the presence of one or several Al-Fe intermetallic phases at the interface between aluminum and iron as well as the absence of

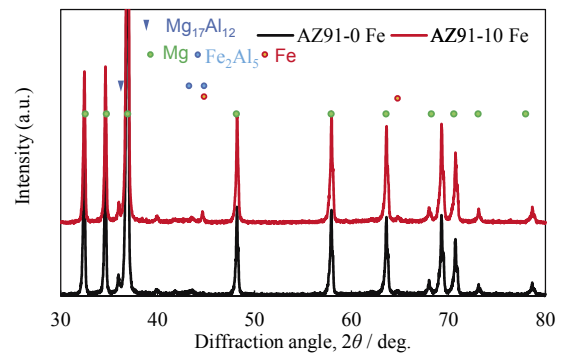


Fig. 4 XRD patterns of AZ91-0 wt. % Fe and AZ91-10 wt. % Fe forged composites.

Kirkendall voids due to inter-diffusion, both indicating that the undissolved iron particles and the magnesium matrix are well metallurgically bonded. Figure 4 compares the XRD spectra of iron-free AZ91 with that of the AZ91 - 10 wt. % Fe forged composite to help determine the one or several intermetallic phases. X-ray diffraction clearly reveals the presence of Al₂Fe₅, as well as a decrease in aluminum solid solution in magnesium identified by a shift to the right of the magnesium peaks [10]. This simply infers that the aluminum solid solution in proximity to the iron particles is slightly reduced, as was already observed by independent EDS measurements (not shown).

Compressive stress-strain curve of iron-free AZ91 and AZ91-10 wt. % Fe forged composite are displayed in Figure 5. First note that the stress vs. strain curves for both the two materials are nearly identical, even though the addition of 10 wt. % iron did cause a slight reduction in yield and ultimate strengths. For the AZ91-10 wt. % Fe forged composite, average yield and ultimate strength were 216 MPa and 475 MPa, respectively, compared to 210 MPa and 484 MPa for the iron-free AZ91. Further, no difference in Vickers micro hardness (HV0.01) was observed between the various materials, another indication that the addition of iron to AZ91 is almost inconsequential to the mechanical properties.

With the mechanical properties now established, test samples were evaluated for corrosion in 3.5 mass% potassium chloride (KCl) solution at 303 deg. K. Figure 6 shows such test samples following 24 hrs exposure to the salt electrolytic solution. The test sample of AZ91 - 10 wt. % Fe most severely corroded. Its weight was reduced from 2.85 grams down to 0.06 grams in 24 hrs compared to no measurable weight change in the iron-free AZ91 test sample, an indication that iron is extremely effective in increasing corrosion rate in AZ91. Surface potential distributions nearby iron particles, as measured by SKPFM, are presented in Figure 7 for the AZ91-1 wt. % Fe forged composite. The difference in surface potential between the AZ91 matrix and the iron was found to be 1.20V compared to 1.05 V between the AZ91 matrix and the Fe- Al intermetallic phase. Both iron particles and Al-Fe intermetallic phase therefore lead to a strong

Materials Design for Corrosion Rate Control in PM AZ91 Mg Alloy by Fe Addition

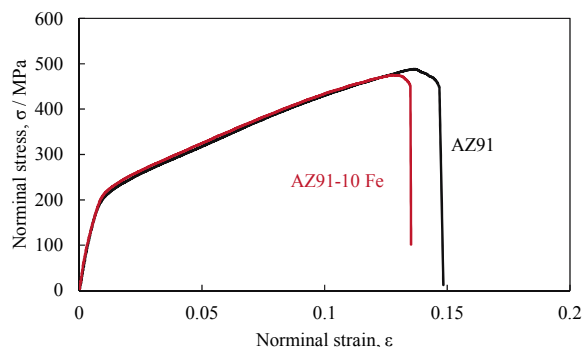


Fig. 5 Stress strain curve of AZ91-0 wt. % Fe and AZ91-10 wt.% Fe Forged composites.


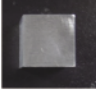


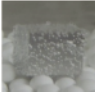


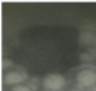

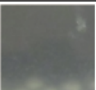



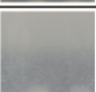

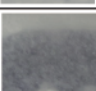
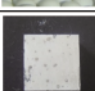

	AZ91-0 Fe	AZ91-10 Fe
Before test	 2.90 g	 2.85 g
0 min		 Alumina ball
30 min		
60 min (1 hr)		
180 min (3 hr)		
360 min (6 hr)		
720 min (12 hr)		
1440 min (24 hr)		
After test	 2.90 g	 0.06 g

Fig. 6 Appearance changes in AZ91-0 wt.% Fe and AZ91- 10 wt.% Fe forged composites during KCl solution immersion test.

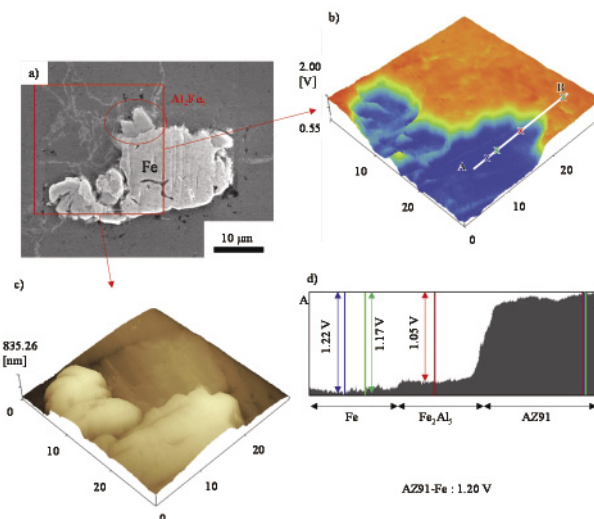


Fig.7 SEM observation on Fe particle of AZ91-10 wt.% Fe forged composite (a), surface potential map at the interface between AZ91 and Fe (b), height map (c) and cross section view of surface potential measured along line A-B (d).

galvanic coupling with the AZ91 magnesium matrix. Calculated corrosion rates for the iron-free AZ91, AZ91 with 0.1, 0.5, and 1 wt. % Fe forged composites are shown in Figure 8. First note that corrosion rate increased significantly with 1 wt. % Fe addition. Published studies on galvanic corrosion of magnesium indicate that foreign particles in magnesium do exhibit a galvanic corrosion circle [11]. AZ91 - 1 wt. % Fe forged composite immersed in 3.5 wt. % KCl solution for 10 min was specifically seen to exhibit an average galvanic corrosion radius of 112 μm . The distance between Fe particles of iron-free AZ91 and AZ91 enriched with 0.5 and 1 wt. % Fe forged composites were 778, 438 and 222 μm . Figure 9 shows average corrosion depth from initial surface of iron-free AZ91 as well as AZ91 with 0.1, 0.5 and 1 wt. % Fe. It may be seen that corrosion depth increases over time and that corresponding rate of increase is essentially determined by the iron content in the alloy composite.

Figure 10 is a schematic representation attempting to depict the corrosion mechanism of the iron-containing AZ91 forged composites for two cases: (a) distant iron particles, and (b) nearby iron particles. In Figure 10, galvanic corrosion is pointed out by the superimposed circles, also depicting the location of iron particles. Corrosion preferably develops in the magnesium matrix surrounding the iron particles. Once enough magnesium has been corroded, the more cathodic iron particles (A) eventually fall and the galvanic corrosion cycle is interrupted, restarting elsewhere at the surface of the material wherein other iron particles are present. After hidden particle (B) are exposed to solution due to galvanic corrosion of first particle (A), matrix around particle (B) is galvanic corroded. It caused the significant increase of corrosion rate of AZ91-1 wt. % Fe forged composite. Short interparticle distance increased corrosion rate of AZ91-1 wt. % Fe. This means that the

corrosion rate of AZ91 composite can be controlled by addition of Fe.

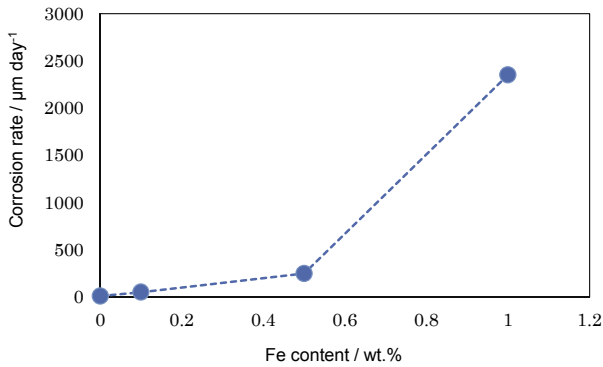


Fig. 8 Relationship between corrosion rate and Fe content of AZ91 forged composites.

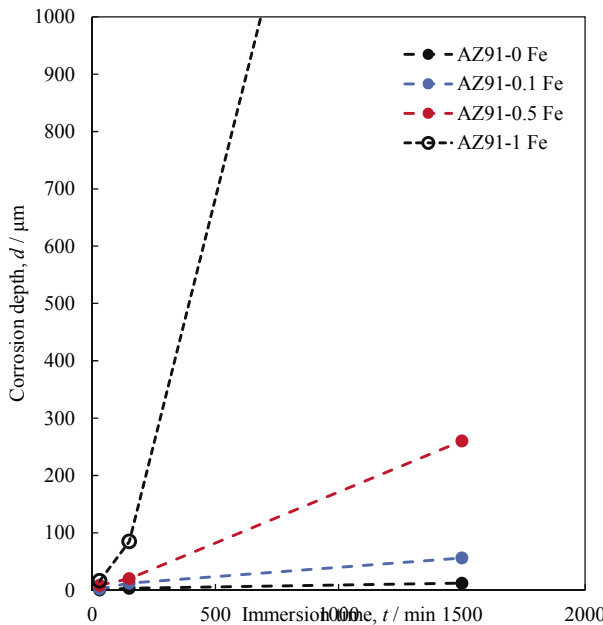


Fig. 9 Dependence of corrosion depth on Fe content of AZ91-Fe forged composites after 3.5% KCl solution immersion test.

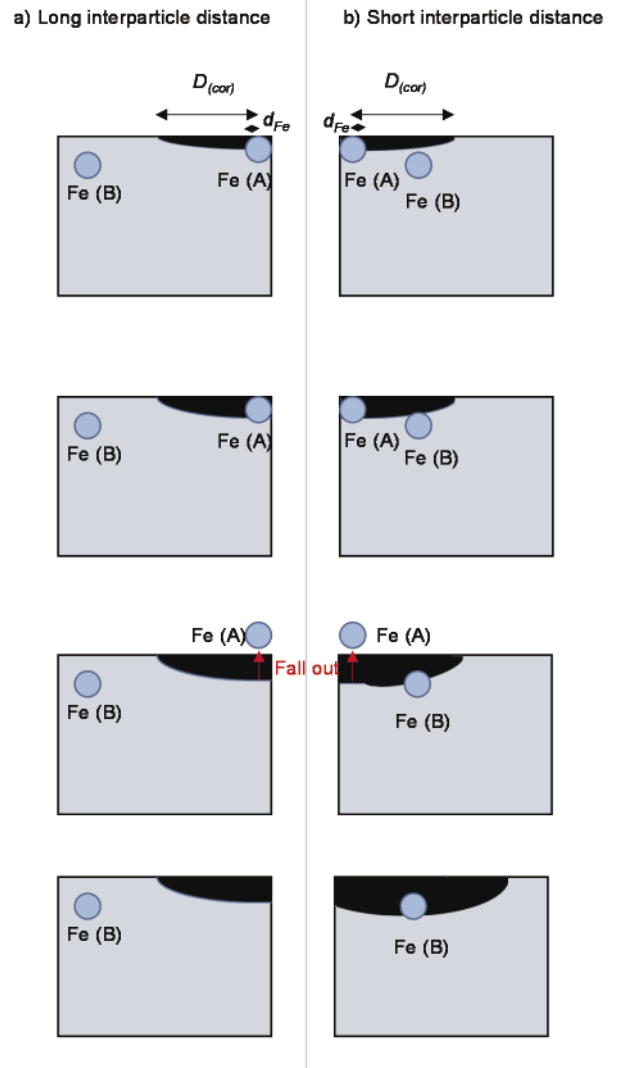


Fig. 10 Schematic illustration of corrosion behavior of AZ91-Fe forged composites with long interparticle distance (a) and short interparticle distance (b).

4. Conclusion

This study establishes that the iron particle, purposely added to AZ91 via powder metallurgy route, is an effective corrosion accelerator. The findings may be summarized as follow:

1. Iron addition to AZ91 does not noticeably influence grain size, microstructure, and micro-hardness. Further, iron-free AZ91 and AZ91 - 10 wt. % Fe forged composites have similar mechanical properties in compression.
2. Corrosion rates of AZ91 may be greatly accelerated through the addition of iron, in particular with iron in excess of 0.5 wt. % Fe.

Materials Design for Corrosion Rate Control in PM AZ91 Mg Alloy by Fe Addition

Acknowledgements

This research is the result of a short research program with Schlumberger Technology Corporations, USA. The authors would like to thank Schlumberger Kabushi Kaisha (Japan) for helping in setting up this project and facilitate the coordination of the efforts.

References

- [1] Eileen De Guire, Shale Gas Recovery - Engineering a Big Business, Bulletin, 2014 (93), 27-35.
- [2] National Energy Board, A Primer for Understanding Canadian Shale Gas - Energy Briefing Note, Energy Briefing Note, 2009.
- [3] Herschel McDivitt, Hydraulic Fracturing 101, Indiana Division of Oil and Gas, 2013.
- [4] D. F. Miner, J.B. Seastone, Handbook of Engineering Materials, Wiley, New York, (1955).
- [5] Hanawalt, J. D., Nelson C. E., and Peloubet J. A., Corrosion Studies of Magnesium and Its Alloys, Transactions of AIME, 1994 (147), 273.
- [6] Davis, J. R., Metals Handbook 2nd Edition, 1998, ASM International.
- [7] G. Song, B. Johannesson, S. Hapugoda, D. St.John, Corros. Sci., 46 (2004) 955-977.
- [8] C. Carraro, R. Maboudian, L. Magagnin, Surface Science Reports, 62 (2007) 499-525.
- [9] S. Bilouk et al., Microelectronic Engineering, 86 (2009) 2038-2044.
- [10] Masanori Kato, Sen Kaiseki (X-ray diffraction), Uchida Rokakuho, 6 (2002).
- [11] Hiroya Shimizu, Graduation thesis of Osaka University, 2014.